PAPER

Check for updates

Synthesis and characterization of new composite from modified silica-coated MnFe₂O₄ nanoparticles for removal of tetracycline from aqueous solution

Alireza Banaei,[a] Afshin Saadat, [ID]*[b] Negar Gharibzadeh[a]
and Parinaz Pargol Ghasemi [ID][a]

In this study, a new composite from silica coated MnFe₂O₄ nanoparticles, diethylenetriamine, 3-chloropropyl trimethoxysilane and Mg–Al Layered Double Hydroxide (Mg–Al LDH/DETA/CPTMS/SCNPs) composite was synthesized. The Mg–Al LDH/DETA/CPTMS/SCNPs composite was examined by Fourier transform infrared spectrometer (FT-IR), Scanning Electron Microscopy (SEM), Energy Dispersive X-ray (EDS), X-ray diffraction (XRD), Thermogravimetric Analysis (TGA) and Vibrating Sample Magnetometry (VSM). The synthesized composite exhibited magnetic property with a saturation magnetization of 0.40 emu g⁻¹. The Mg–Al LDH/DETA/CPTMS/SCNPs composite was utilized as a successful adsorbent for removal of tetracycline from aqueous solutions. The effect of various operation factors such as initial drug concentration, adsorbent dosage, pH and contact time were investigated. The optimized variable conditions such as adsorbent dose of 60 mg L⁻¹, drug concentration of 100 mg L⁻¹, pH = 7 and contact time 30 min were obtained. For describing the adsorption isotherms, the Langmuir, Freundlich and Temkin adsorption models were utilized. The results indicated that the adsorption isotherm is in good agreement with Langmuir model. According to the Langmuir analysis, the maximum adsorption capacity (q_m) of the Mg–Al LDH/DETA/CPTMS/SCNPs composite for tetracycline was obtained to be 40.16 mg g⁻¹. The kinetic studies revealed that the adsorption in all cases to be a pseudo second-order process. The negative value of $\Delta G°$ and the positive value of $\Delta H°$ showed the adsorption process to be spontaneous and endothermic.

1. Introduction

In the current era, the use of organic compounds in various industries such as food and medicine and the release of their effluents into surface and groundwater has become a serious threat to the health of the environment and humans. Wastewaters contain a number of pollutants such as antibiotics, dyes, pesticides, phenols, *etc.*, which are highly toxic and difficult to degrade *via* chemical, biological, and photolytic processes.[1] In this field, antibiotics are one of the most toxic constituents of industrial wastes. Most of the antibiotics in the human and animal body enter the environment without being metabolized as active compounds through urine and feces.[2] Other sources of drug pollutants include the discharge of expired drugs, agricultural and veterinary waste, as well as the discharge from laboratory and research activities.[3] One of the most widely used

antibiotics in the world is tetracycline, which accounts for more than one-third of the total antibiotic production and consumption.[4] Tetracycline has high antimicrobial activity against Gram positive and negative bacteria because of its aromatic structure that contains the naphthol chemical group.[5,6] The chemical structure of this antibiotic is shown in Fig. 1. In some studies, the amount of tetracycline in surface water and in the wastewater of hospitals and pharmaceutical factories are reported 2–0.38 mg L⁻¹ and 100–500 mg L⁻¹, respectively. The presence of tetracycline in water sources causes impaired fertility, chronic toxicity, allergic reactions, headache and visual disturbances, diarrhea and vomiting.[7] Based on this, the need for an efficient system to remove tetracycline from the aqueous environment is felt. Several methods can be used for treating wastewater such as biological treatment, photodegradation, nanofiltration, precipitation, osmosis, coagulation, flocculation, distillation and adsorption.[1] However, most of the above mentioned methods are ineffective due to factors such as operational costs, secondary wastes, environmental effects and related problems, efficiency and applications.[8] In recent years, the adsorption process has been widely used due

[a]Department of Chemistry, Payame Noor University, P. O. Box 19395-3697, Tehran, Iran

[b]Department of Chemistry, Germi Branch, Islamic Azad University, Germi, Iran. E-mail: Afshin.Saadat@iau.ac.ir

to its simple design, being inexpensive, ease of management, high efficiency, ability to regenerate the adsorbent, and compatibility with the environment.[9,10] The features of the adsorbate such as ionic charge, hydrophobicity, size and polarity and also physicochemical properties such as morphology, specific surface area and surface polarity determine the effectiveness of the adsorption process.[11] Recently, nanocomposites have been widely used in various industries such as water treatment, agriculture and pharmaceuticals industries *etc.*[12–17] In the field of water treatment, various nanocomposites are used for the purification of industrial wastewater *via* economically efficient adsorption process.[18] Ahamad *et al.* used chitosan based magnetic nanocomposite for removal of tetracycline from aqueous solution.[19] Li *et al.* prepared NiFe$_2$O$_4$–COF–chitosan–terephthalaldehyde nanocomposite and used it for removal of tetracycline.[6] In the other work, Shao *et al.* synthesized MnFe$_2$O$_4$/activated carbon magnetic composites for removal of tetracycline. The result showed this nanocomposite had excellent performance for removal of tetracycline.[20] Recent research indicated that LDH hybrids are good multifunctional materials for applying in different applications such as energy storage, photo-catalysis and as nanocomposites in water purification.[21] Some important properties of LDH are thermal stability, alkalinity and adjustability resulted from its unique structure which also provides it with an excellent adsorption capacity.[22] LDHs, formed from positively charged hydroxide metal sheets and water molecules and internal anions, have been widely studied as favorable tetracycline adsorbents.[23–25] In this work, new Mg–Al LDH/DETA/CPTMS/SCNPs composite was prepared (Scheme 1). The synthesized composite was used for the removal of the tetracycline from water solution. Moreover, the effects of various factors such as initial drug concentration, adsorbent dosage, contact time and pH on adsorption behavior were investigated. Adsorption isotherms, kinetics and thermodynamic studies have been reported to account for the nature of adsorption process.

2. Materials and methods

2.1. Chemicals and reagents

Ferric chloride hexahydrate (FeCl$_3$·6H$_2$O) and manganese sulfate (MnSO$_4$·H$_2$O) with 98% purity, sodium hydroxide (NaOH) with 98% purity and ammonia (NH$_3$) with 25% purity were purchased from Merck, Germany. Tetraethyl orthosilicate (TEOS), diethylenetriamine and 3-chloropropyl trimethoxysilane with 99% purity were purchased from Merck. Tetracycline hydrochloride were purchased from Sigma-Aldrich.
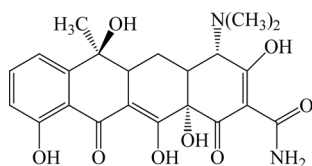

Fig. 1 Chemical structure of tetracycline.

2.2. Instrumentation

FT-IR spectra (Shimadzu Prestige-21) were applied to record the identity of the as prepared composite. All absorption spectra were recorded in the range of 400–4000 cm^{-1} using KBr pellets at room temperature. The crystal structure of the synthesized adsorbent was analyzed by performing X-ray diffraction (XRD) on Bruker D8 ADVANCE X-ray diffractometer with Cu Kα radiation ($\lambda = 1.5418$ Å) operated at 40 kV and 40 mA. The average size of composite particles is also estimated *via* Debye–Scherrer (eqn (1)):[26]

$$D = \frac{K\lambda}{\beta \cos \theta} \qquad (1)$$

where D is the average size, λ is the X-ray source wavelength (1.54 Å), β is the full width at half maximum (FWHM) of the diffraction peak and θ is the Bragg's angle. The surface morphology of the synthesized compounds was recorded with a scanning electron microscope (LECO SEM, Michigan, USA). Magnetic measurements were done by vibrating sample magnetometry method, using a VSM 7407 magnetometer, at ambient temperature. The thermal stability of sample was verified thermogravimetric analysis (TGA), conducted at Linseis (STA PT 1600) thermogravimetric analyzer from 20 °C to 800 °C under N$_2$ atmosphere with heating rate of 20 °C min^{-1}. UV-visible spectra in the 200–1000 nm range were gained in DMF solvent on a PerkinElmer Lambda 45 spectrophotometer. A Jenway model 4510 pH-meter was used for pH measurements by use of a combined electrode. A Hielscher UP 400S ultrasonicator with an operating voltage of 450 V was used to disperse the nanoparticles in solution. The magnetic separation was done by a strong magnet with 1.4 T magnetic fields (5 cm × 4 cm × 2 cm).

2.3. Preparation of the MnFe$_2$O$_4$@SiO$_2$@CPTMS@DTAM@Mg/Al-LDH composite

2.3.1. Preparation of manganese ferrite nanoparticles (NPs). MnFe$_2$O$_4$ nanoparticles were synthesized using the typical co-precipitation process according to with minor changes.[27] For this aim, FeCl$_3$·6H$_2$O (1.8 g) and MnSO$_4$·H$_2$O (2.55 g) were dissolved in 150 mL deionized water under N$_2$ gas with stirring at 80 °C. In the next step, sodium hydroxide 8 M was added slowly to the solution to raise the pH to 10. After 3 h magnetic stirring, MnFe$_2$O$_4$ nanoparticles precipitates was separated by a magnetic separation and then washed with ethanol and deionized water. The MnFe$_2$O$_4$ nanoparticles were dried at 60 °C for 24 h.

2.3.2. Synthesis of silica-coated nanoparticles (SCNPs). The silica-coated nanoparticles (SCNPs) were prepared according to the previous report.[28] The MnFe$_2$O$_4$ suspension prepared above (6 g) was dispersed in a 250 mL round-bottom flask containing 100 mL of 0.1 M HCl aqueous solution. Then, solution ultrasonically agitated for 20 minutes. Nanoparticles isolated and washed with deionized water. In the next step, the nanoparticles were added to solution containing 40 mL deionized water, 100 mL ethanol and 15 mL 28% ammonia aqueous solution and stirred for 30 min. Then 20 mL tetraethylorthosilicate (TEOS) in
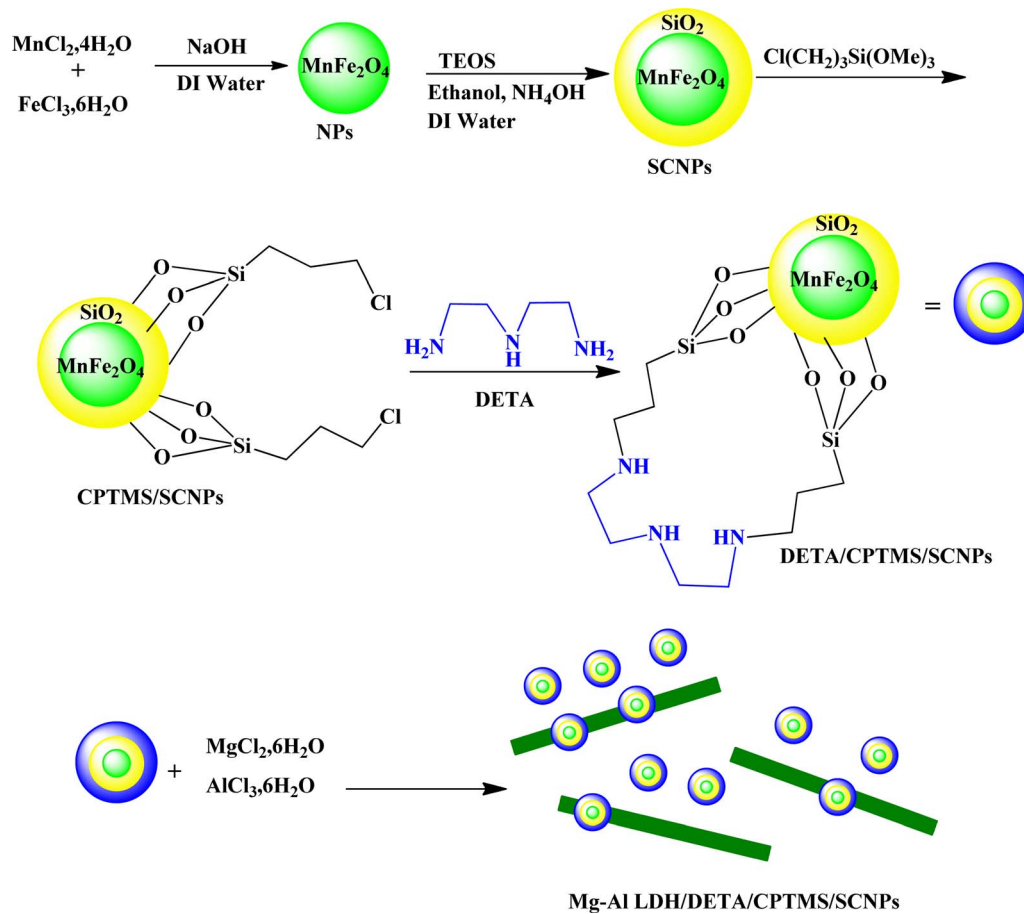
Scheme 1 The synthesis route of Mg–Al LDH/DETA/CPTMS/SCNPs composite.

20 mL ethanol was added to solution. The solution was stirred for 8 h at room temperature. Finally, the product was magnetically separated and washed with deionized water and ethanol.

2.3.3. Synthesis of silica-coated nanoparticles modified with 3-chloropropyl trimethoxysilane (CPTMS/SCNPs). SCNPs (2 g) and 60 mL 3-chloropropyl trimethoxysilane were placed in 50 mL dry toluene. The mixture was stirred for 48 h at 60 °C under N_2 gas. The CPTMS/SCNPs was separated by magnetic separation and washed with toluene and ethanol and dried under vacuum at 80 °C.

2.3.4. Synthesis of CPTMS/SCNPs bonded diethylenetriamine (DETA/CPTMS/SCNPs). To a mixture of CPTMS/SCNPs (2 g) in 50 mL dry toluene, 60 mL diethylenetriamine was added. Then, the mixture was stirred at reflux for 48 h under N_2 gas. The reaction was cooled to room temperature and the product was separated by magnetic separation and washed with methanol and toluene and dried under vacuum at 80 °C.

2.3.5. Synthesis of (Mg–Al LDH/DETA/CPTMS/SCNPs) composite. For this aim Mg–Al LDH were prepared through coprecipitation-hydrothermal treatment method reported previously.[29] 10 mL of $AlCl_3 \cdot 6H_2O$ (0.1 M) and $MgCl_2 \cdot 6H_2O$ (0.3 M) were mixed in a 150 mL round-bottom flask. Then, the mixture was stirred for 30 min stirrer at room temperature. In the next step, 40 mL sodium hydroxide (0.15 M) was added to

solution and stirred for 15 min. The product was transferred to an autoclave and heated in an oven at 100 °C for 24 h. The mixture was transferred to 100 mL round-bottom flask containing 50 mL ethanol. Then, DETA/CPTMS/SCNPs (1 g) was placed into the reaction contents and stirred for 20 h. Finally, the suspension was aged at 60 °C for 24 h and precipitates were collected by magnetic separation, washed with ethanol and deionized water and dried under vacuum.

2.4. Adsorption experiments

Synthesized composite (Mg–Al LDH/DETA/CPTMS/SCNPs) was used removal of tetracycline from aqueous solutions by batch technique. Experiment parameters such as pH value (2–11), drug concentration (10–120 mg L^{-1}), adsorbent dosage (0–100 mg) and contact time (10–50 min) on the adsorption of tetracycline in aqueous solution were studied in detail. For conducting the experiments, solution of 1000 mg L^{-1} of tetracycline was prepared in deionized water and diluted to obtain the desired concentrations of drug. All concentrations of tetracycline in water solutions were studied by the ultraviolet visible (UV-Vis) method at 277 nm. The amount of the tetracycline adsorbed onto adsorbent (q_e in mg g^{-1}) and the percentage of the tetracycline removed from the solution (R in %) were calculated from the eqn (2) and (3):

$$q_e = \frac{(C_0 - C_e)}{M} \times V \tag{2}$$

$$R\ (\%) = \frac{(C_0 - C_e)}{C_0} \times 100 \tag{3}$$

where, C_0 and C_e are the initial and equilibrium concentration of drug in solution (mg L^{-1}), respectively. V is the initial volume of the drug solution (L) and M is the mass of adsorbent used (g).

3.   Results and discussion

3.1.   Preparation of Mg–Al LDH/DETA/CPTMS/SCNPs composite

In this study, two-steps method was used for the preparation of Mg–Al LDH/DETA/CPTMS/SCNPs composite. First, the DETA/CPTMS/SCNPs nanoparticles were prepared *via* reaction of SCNPs nanoparticles, 3-chloropropyl trimethoxysilane and diethylenetriamine. Then, DETA/CPTMS/SCNPs nanoparticles were mixed with Mg–Al LDH. The preparation route of Mg–Al LDH/DETA/CPTMS/SCNPs adsorbent is shown in Scheme 1. The prepared composite was characterized by FI-IR, SEM, EDS, XRD, TGA and VSM. Finally, the composite was applied as an efficient adsorbent for removal of tetracycline from aqueous solutions by batch method.

3.1.1.   Fourier transform infrared spectroscopy analysis (FT-IR). The FT-IR spectra of prepared compounds are shown in Fig. 2. The spectrum of Fig. 2a is related to the of NPs. As observed, the NPs spectrum showed stretching vibrations at 3429 and 1627 cm^{-1} which assigned to the stretching and bending vibration of hydroxyl (OH) groups. Furthermore, the absorption bands at 1114 and 613 cm^{-1} which were corresponded to bonded hydroxyl groups on the metal and octahedral and tetrahedral metal-oxide (Fe–O) bond stretching vibration modes, respectively.[30,31] The FT-IR spectrum of SCNPs (Fig. 2b), after reaction with TEOS showed a new peak at 1076 cm^{-1} is attributed to stretching vibration of Si–O–Si. Fig. 2c demonstrated a new peak at 796 cm^{-1} due to C–Cl bond.[32] In comparison with CPTMS/SCNPs (Fig. 2c), the FT-IR spectrum of the DETA/CPTMS/SCNPs (Fig. 2d) demonstrated a disappearance of the adsorption peak at 796 cm^{-1} and the formation of a new peaks at 3414, 2920 and 1448 resulted from stretching vibrations N–H, C–H and C–N bands, respectively.[33] Fig. 2d and e demonstrate the FT-IR spectra of Mg–Al LDH and Mg–Al LDH/DETA/CPTMS/SCNPs composite, respectively. In FTIR spectrum of synthesized composite, a broad peak at 3427 cm^{-1} belongs to the stretching vibration of the interlayer water molecules in the Mg–Al LDH. Furthermore, the strong peak observed at 1631 cm^{-1} corresponds to the vibration hydroxyl deformation mode of the water. The absorption peaks at 598 and 454 cm^{-1} is related to the lattice vibration of Al–O and Mg–O bonds, respectively.[34,35]

3.1.2.   X-ray diffraction (XRD). X-ray diffraction of Mg–Al LDH/DETA/CPTMS/SCNPs composite are shown in Fig. 3. The XRD peaks of NPs could be seen at $2\theta = 30.20°$ (220), 35.45° (311), 43.25° (400), 53.50° (422), 57.15° (511) and 63.40° (533), and (64), showing the spinel crystal structure of NPs, which are
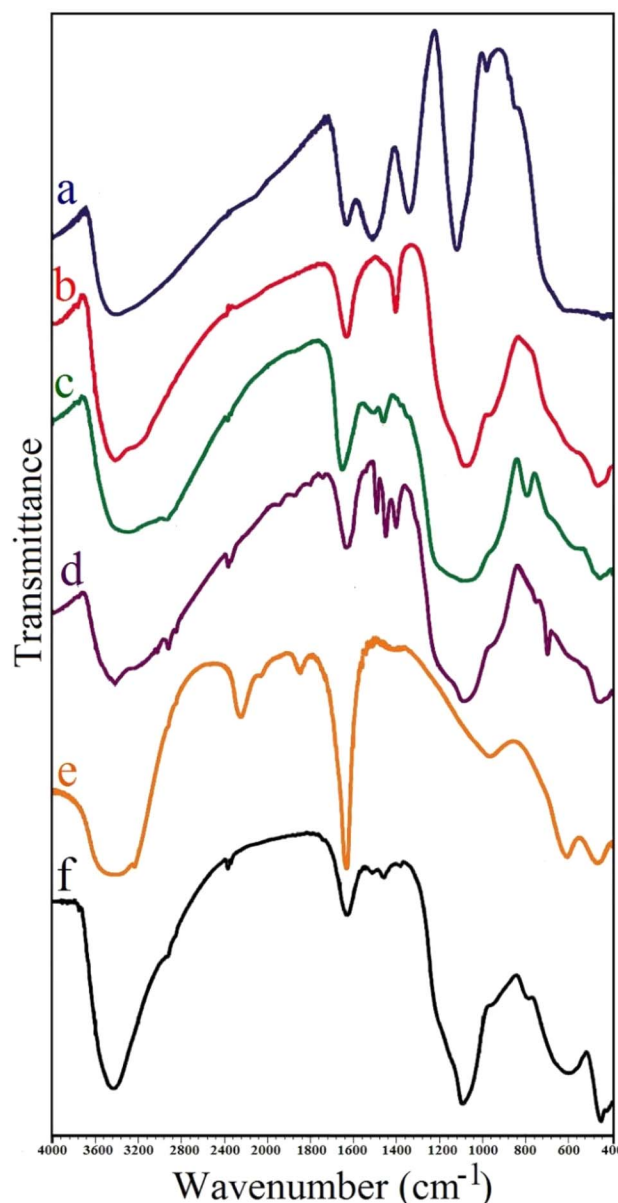

Fig. 2 FT-IR spectra of (a) NPs, (b) SCNPs, (c) CPTMS/SCNPs, (d) DETA/CPTMS/SCNPs, (e) Mg–Al LDH and (f) Mg–Al LDH/DETA/CPTMS/SCNPs composite. Reaction conditions: (a) FeCl$_3$·6H$_2$O (1.8 g), MnSO$_4$·H$_2$O (2.55 g), deionized water (150 mL), under N$_2$ gas, NaOH 8 M, pH 10, 80 °C, 3 h. (b) MnFe$_2$O$_4$ (6 g), 0.1 M HCl (100 mL), ultrasonic irradiation, 40 mL deionized water, ethanol (100 mL), 28% ammonia aqueous solution (15 mL), TEOS (20 mL), r.t., 8 h. (c) SCNPs (2 g), 3-chloropropyl trimethoxysilane (60 mL), dry toluene (50 mL), under N$_2$ gas, 60 °C, 48 h. (d) CPTMS/SCNPs (2 g), dry toluene (50 mL), diethylenetriamine (60 mL), under N$_2$ gas, 48 h. (e) 0.1 M AlCl$_3$·6H$_2$O (10 mL), 0.3 M MgCl$_2$·6H$_2$O (10 mL), 0.15 M NaOH (40 mL), autoclave, 100 °C, 24 h. (f) Mg–Al LDH, DETA/CPTMS/SCNPs (1 g), 60 °C for 24 h.

in agreement with the referenced data for NPs.[36] Besides, the dominant peaks of Mg–Al LDH/DETA/CPTMS/SCNPs composite appeared at $2\theta = 11.67°$, 23.50°, 35.50°, 43.30°, 57.91° and 63.50°. The new peaks at $2\theta = 11.67°$ (003) and 23.50° (006) were attributed to Mg–Al LDH.[37] As it can be observed in Fig. 3, after
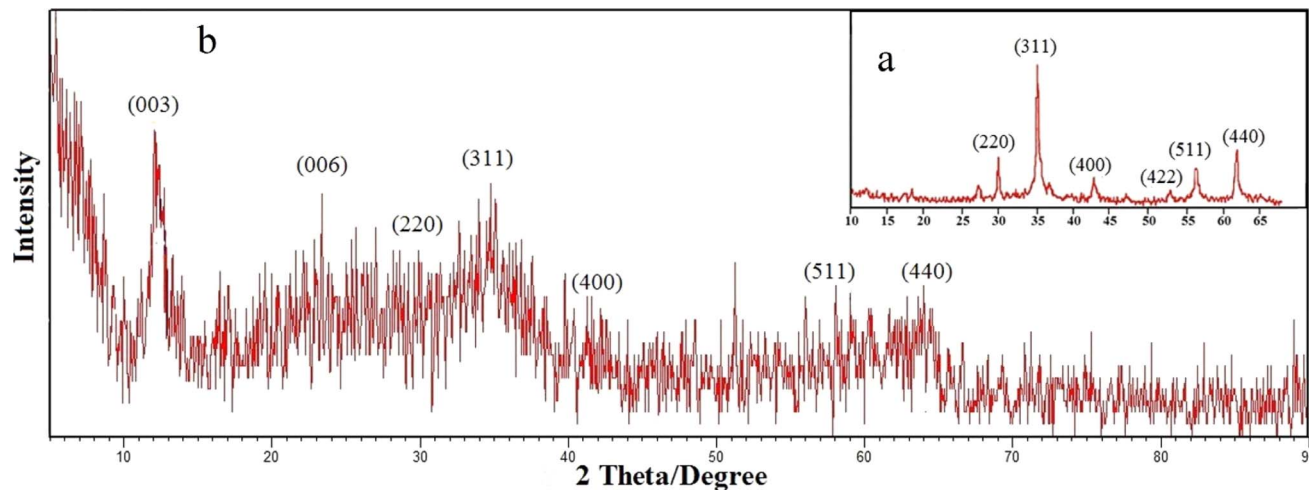
Fig. 3 XRD pattern of (a) $MnFe_2O_4$, (b) Mg–Al LDH/DETA/CPTMS/SCNPs composite. Reaction conditions: (a) $FeCl_3 \cdot 6H_2O$ (1.8 g), $MnSO_4 \cdot H_2O$ (2.55 g), deionized water (150 mL), under N_2 gas, NaOH 8 M, pH 10, 80 °C, 3 h. (b) 0.1 M $AlCl_3 \cdot 6H_2O$ (10 mL), 0.3 M $MgCl_2 \cdot 6H_2O$ (10 mL), 0.15 M NaOH (40 mL), autoclave, 100 °C, 24 h, DETA/CPTMS/SCNPs (1 g), 60 °C, 24 h.

the grafting of layers on the surface of $MnFe_2O_4$ NPs, although the peaks intensity is weaker than that of magnetic $MnFe_2O_4$ NPs, all of the peaks related to pure $MnFe_2O_4$ NPs could be observed. According to the Debye–Scherrer equation, the particles size of the Mg–Al LDH/DETA/CPTMS/SCNPs composite was 153 nm.

3.1.3. Scanning electron microscopy (SEM). SEM was utilized to determine the morphology and size of different samples. Fig. 4 shows SEM images of synthesized compounds, which demonstrating that the products are all well-dispersed with spherical morphology. The SEM image showed that NPs have an average particle size of 48 nm (Fig. 4a). After coating with a silica layer, the SCNPs nanoparticles was obtained with an average size of 62 nm (Fig. 4b). Subsequently, Fig. 4c and d represent SEM images of SCNPs modified with 3-chloropropyl trimethoxysilane and diethylenetriamine, respectively. The size of CPTMS/SCNPs and DETA/CPTMS/SCNPs are relatively uniform and the average particle size are 71 and 87 nm respectively. Fig. 4e displays the SEM micrograph of Mg–Al LDH/DETA/CPTMS/SCNPs composite. According to the SEM image the average size of the nanocomposite is 239 nm. The chemical composition of Mg–Al LDH/DETA/CPTMS/SCNPs composite was investigated through EDS analysis. As shown in Fig. 5, EDS measurement confirmed that the composite contains C, N, O, Mg, Al, Si, Mn and Fe.

3.1.4. Thermogravimetric analysis (TGA). TGA and DTG analysis were also done to evaluate the thermal stability of Mg–Al LDH/DETA/CPTMS/SCNPs composite in the range of 50–700 °C. The TGA and DTG curves of composite is shown in Fig. 6. The first weight loss (4%) at 50–100 °C is caused by the evaporation of surface water molecules and solvent adsorbed on the of Mg–Al LDH/DETA/CPTMS/SCNPs composite.[38,39] The second weight loss at 150–450 °C (18%) are attributed to the thermal decomposition of Mg-Al hydroxide sheets and organic component in Mg–Al LDH/DETA/CPTMS/SCNPs composite.[40] The last stage degradation occurred 450–600 °C with 4% relates

to the carbonate decomposition in the interlayers and recrystallization.[41] The residual mass of the Mg–Al LDH/DETA/CPTMS/SCNPs composite was 74%.

3.1.5. Magnetization analysis (VSM). The magnetic behavior of synthesized compounds was verified by vibrating sample magnetometry (VSM) in the range between 15 000 and −15 000 Oe. As showed in Fig. 7, the magnetization saturation values for NPs, SCNPs, CPTMS/SCNPs, DETA/CPTMS/SCNPs and Mg–Al LDH/DETA/CPTMS/SCNPs composite were gained as 1.21, 0.80, 0.719, 0.60 and 0.40 emu g^{-1}, respectively. The saturation magnetisation value of composite enables to separate the adsorbent from aqueous solution using an external magnet during magnetic solid phase extraction. The magnetic property of composite is strongly affected by the amount of magnetite nanoparticles. The VSM results show coating the surface of the NPs with SiO_2, 3-chloropropyl trimethoxysilane, diethylenetriamine and Mg–Al LDH results in a decrease in the saturation magnetization. This is due to the presence of nonmagnetic components on the surface of NPs which may produce a layer that is magnetically dead. Therefore, any crystalline disorder within the surface layer leads to a significant decrease in the saturation magnetization of nanoparticles.[42,43]

3.2. Sorption studies of tetracycline

3.2.1. Effect of adsorbent dosage. In the present study, the influence of adsorbent dosage on adsorption removal of tetracycline was studied by using different amounts of sorbent in the range 0–100 mg in the beaker containing 10 mL of drug solution (100 mg L^{-1}) at pH = 7 for 10 min. Fig. 8 illustrates the effect of adsorbent dosage on the percentage removal of drug. It can be observed from Fig. 8 that the percentage removal of tetracycline from the solution increased from 0% to 67% with increasing adsorbent dosage from 0 to 100 mg. An increase in the percentage of tetracycline removal can be related to the increased surface area of the adsorbent and availability of more adsorption sites. The maximum drug removal efficiency has
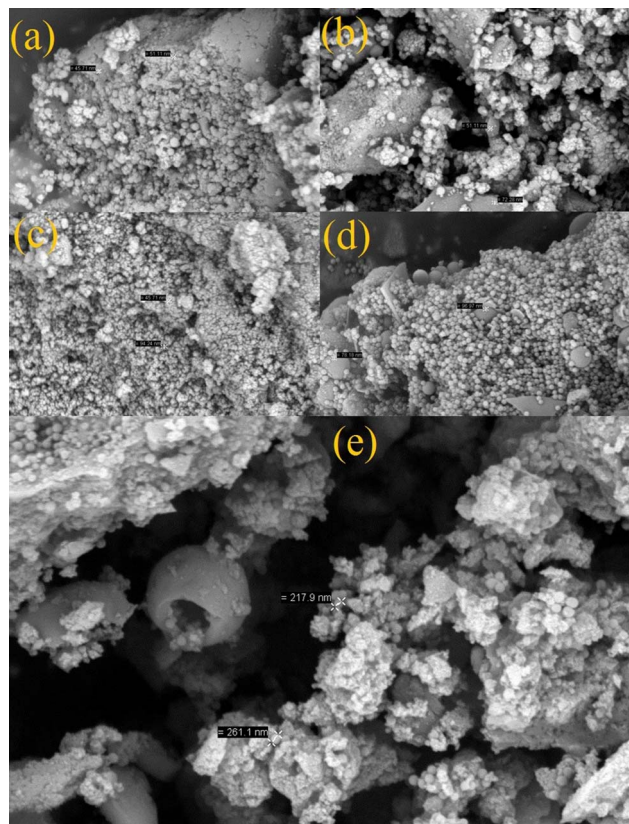
Fig. 4 SEM images of (a) NPs, (b) SCNPs, (c) CPTMS/SCNPs, (d) DETA/CPTMS/SCNPs, (e) Mg–Al LDH/DETA/CPTMS/SCNPs composite. Reaction conditions: (a) $FeCl_3 \cdot 6H_2O$ (1.8 g), $MnSO_4 \cdot H_2O$ (2.55 g), deionized water (150 mL), under N_2 gas, NaOH 8 M, pH 10, 80 °C, 3 h. (b) $MnFe_2O_4$ (6 g), 0.1 M HCl (100 mL), ultrasonic irradiation, 40 mL deionized water, ethanol (100 mL), 28% ammonia aqueous solution (15 mL), TEOS (20 mL), r.t., 8 h. (c) SCNPs (2 g), 3-chloropropyl trimethoxysilane (60 mL), dry toluene (50 mL), under N_2 gas, 60 °C, 48 h. (d) CPTMS/SCNPs (2 g), dry toluene (50 mL), diethylenetriamine (60 mL), under reflux, under N_2 gas, 48 h. (e) 0.1 M $AlCl_3 \cdot 6H_2O$ (10 mL), 0.3 M $MgCl_2 \cdot 6H_2O$ (10 mL), 0.15 M NaOH (40 mL), autoclave, 100 °C, 24 h, DETA/CPTMS/SCNPs (1 g), 60 °C for 24 h.

been gained at 60 mg of the adsorbent. Therefore, for further study, optimum amount 60 mg of Mg–Al LDH/DETA/CPTMS/SCNPs composite were used.

3.2.2. Effect of initial drug concentration. The effect of initial concentration of tetracycline on adsorption of it on Mg–Al LDH/DETA/CPTMS/SCNPs composite were studied in different initial concentrations of tetracycline between 10 and 120 mg L^{-1} with keeping constant the other parameters (pH 7 and adsorbent dose 60 mg). As observed in Fig. 9, the percent of drug removal slightly decreased from around 88% at a concentration of 10 mg L^{-1} to 50% when the concentration was increased to 110 mg L^{-1}. May be, this is because of the unavailability of enough number of active sites of drug molecules for binding on the surface of the adsorbent. According to the findings of Fig. 9, optimum initial concentration of 100 mg L^{-1} was chosen in the adsorption experiment.

3.2.3. Effect of contact time. In this study, the influence of contact time on adsorption of tetracycline on the surface of synthesized composite were investigated at room temperature with the different contacting time at 0–45 min. For all test solutions the initial drug concentrations were 100 mg L^{-1}. As shown in Fig. 10, by increasing the contact time percent adsorption of drug on composite was increased. The adsorption process is relatively rapid within the initial contact time, it can be due to the presence of many empty active sites and functional groups on the adsorbents. Moreover, in the later stages of contact time the rate of the removal became slower, because of the decreasing of active sites. The removal efficiency of drug rapidly increased from 67.52% to 75.52% in 45 min. Therefore, the optimum contact time of composite were selected as 30 min.

3.2.4. Effect of pH solution. The pH is considered as an important factor in the adsorption of drug onto the adsorbent. Since it affects the surface charge of the adsorbent, the degree of dissociation of functional groups of the adsorbent and the structure of the drug molecule.[44] In this work, the experiments were conducted at different pH (2–11) to determine the optimum pH for the removal of drug. For this experiment,
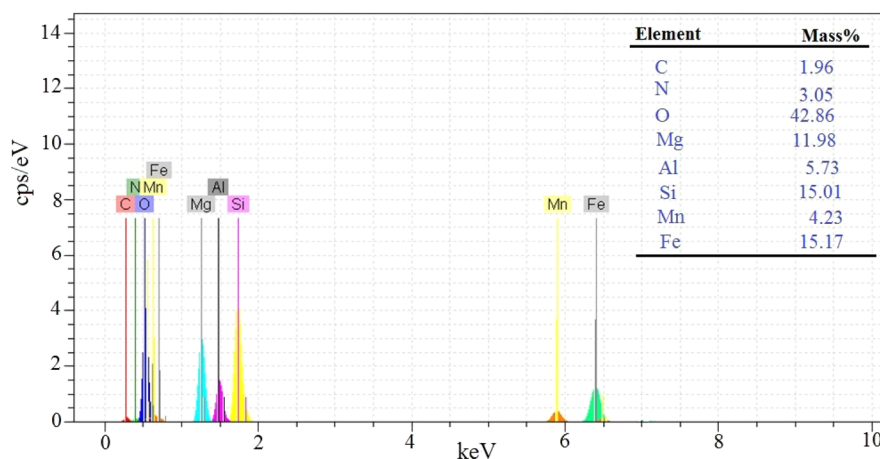

Fig. 5 EDS patterns of Mg–Al LDH/DETA/CPTMS/SCNPs composite. Reaction conditions: 0.1 M $AlCl_3 \cdot 6H_2O$ (10 mL), 0.3 M $MgCl_2 \cdot 6H_2O$ (10 mL), 0.15 M NaOH (40 mL), autoclave, 100 °C, 24 h, DETA/CPTMS/SCNPs (1 g), 60 °C for 24 h.
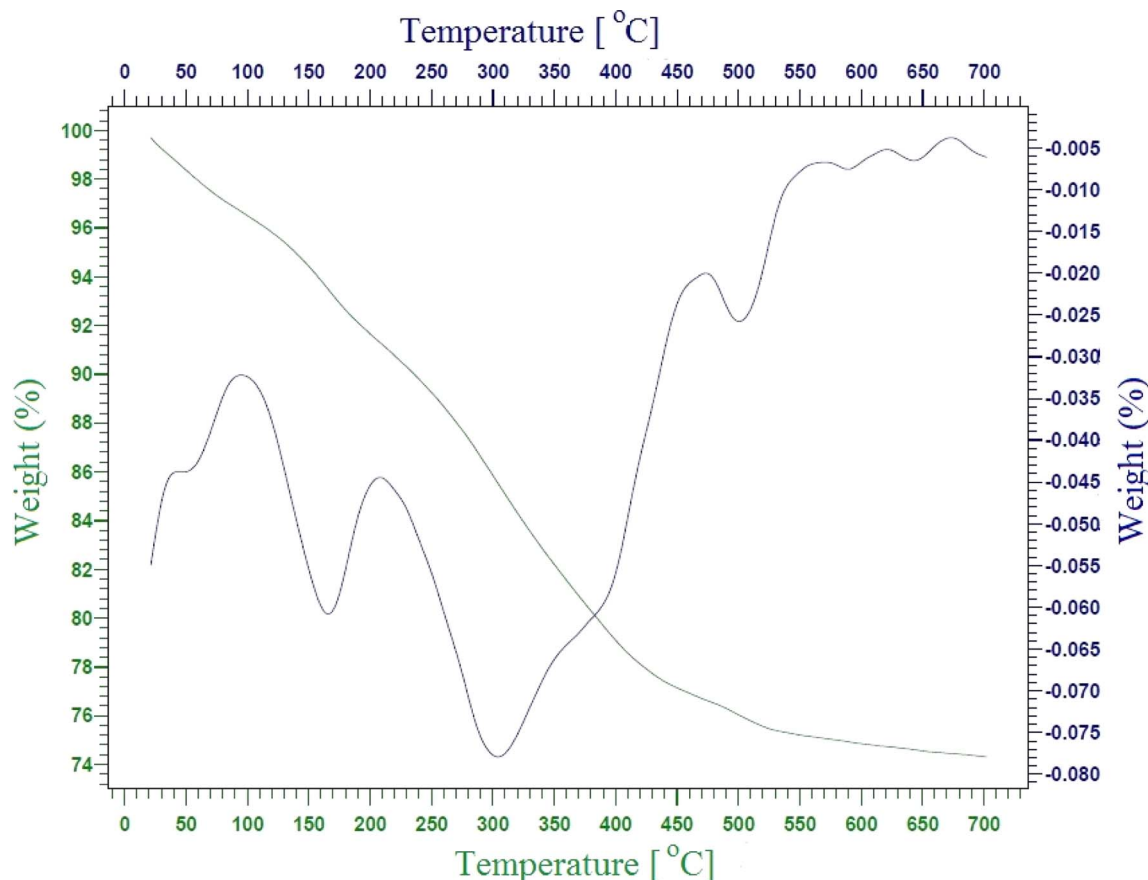
Element	Mass%
C	1.96
N	3.05
O	42.86
Mg	11.98
Al	5.73
Si	15.01
Mn	4.23
Fe	15.17

Fig. 6 TGA curves of the Mg–Al LDH/DETA/CPTMS/SCNPs composite. Reaction conditions: 0.1 M AlCl$_3$·6H$_2$O (10 mL), 0.3 M MgCl$_2$·6H$_2$O (10 mL), 0.15 M NaOH (40 mL), autoclave, 100 °C, 24 h, DETA/CPTMS/SCNPs (1 g), 60 °C for 24 h.

100 mg L^{-1} of solution of drug containing 60 mg adsorbent was used. Beside, 0.1 M HCl and 0.1 M NaOH solutions were used to adjust the pH of the solution. In different pH of the solution, tetracycline has variable charges on different sites (Fig. 11). In pH less than 4, due to the protonation of dimethylammonium group tetracycline exists as a cation. Tetracycline is a zwitterion at the pH between 4 and 7.5 because of the loss of a proton from the phenolic diketone moiety, also tetracycline at pH higher than 7.5 exists as anion because of the loss of a proton from the phenolic di-ketone moiety and tri-carbonyl system.[45] Fig. 12 shows the effect of pH on the percentage removal of drug by composite. By increasing the pH from 2 to 7, the adsorption of tetracycline on composite increases. The maximum adsorption occurs at pH = 7. At acidic condition, tetracycline and composite are mainly of cationic form and adsorption process is not done. With the increasing pH, tetracycline begins to deprotonate. Therefore, the increased adsorption of the drug on the adsorbent above pH = 4 is mainly attributable to the electrostatic attraction between the cationic charged and negatively charged on the tetracycline and Mg–Al LDH/DETA/CPTMS/SCNPs composite. These findings show that, pH = 7 was selected as an optimum pH value for removal of tetracycline from aqueous solution.

3.2.5. Adsorption isotherm. One of the important methods to investigate the relationship between the amount of adsorbed

on adsorbent in the solution phase is adsorption isotherm.[46] To describe the relationship between the adsorbed amount on adsorbent, several isotherm models have been developed.[47] In the present study, various adsorption isotherm models like those of Langmuir, Freundlich and Temkin were applied to evaluating the adsorption of drug from solution. The Langmuir isotherm model is based on the monolayer adsorption of the adsorbate onto the adsorbent surface.[48] The eqn (4) shows the linear form of the Langmuir model:

$$\frac{C_e}{q_e} = \frac{1}{K_L \times q_m} + \frac{C_e}{q_m} \tag{4}$$

where, C_e is the equilibrium concentration of the dye solution (mg L^{-1}), q_e (mg g^{-1}) is the amount of dye adsorbed, q_m is the value of monolayer adsorption capacity in Langmuir model and K_L: constant value of Langmuir (mg L^{-1}). The Langmuir plot for the adsorption of tetracycline onto Mg–Al LDH/DETA/CPTMS/SCNPs composite is shown in Fig. 13. The values of q_m and K_L were calculated from the linear regression plot of (C_e/q_e) *versus* C_e at 25 °C.

The Freundlich isotherm model demonstrates a heterogeneous adsorption of adsorbate onto the adsorbent surface. Eqn (5) shows the linear form of the Freundlich isotherm model:

$$\text{Ln } q_e = \ln K_f + \left(\frac{1}{n}\right)\ln C_e \tag{5}$$
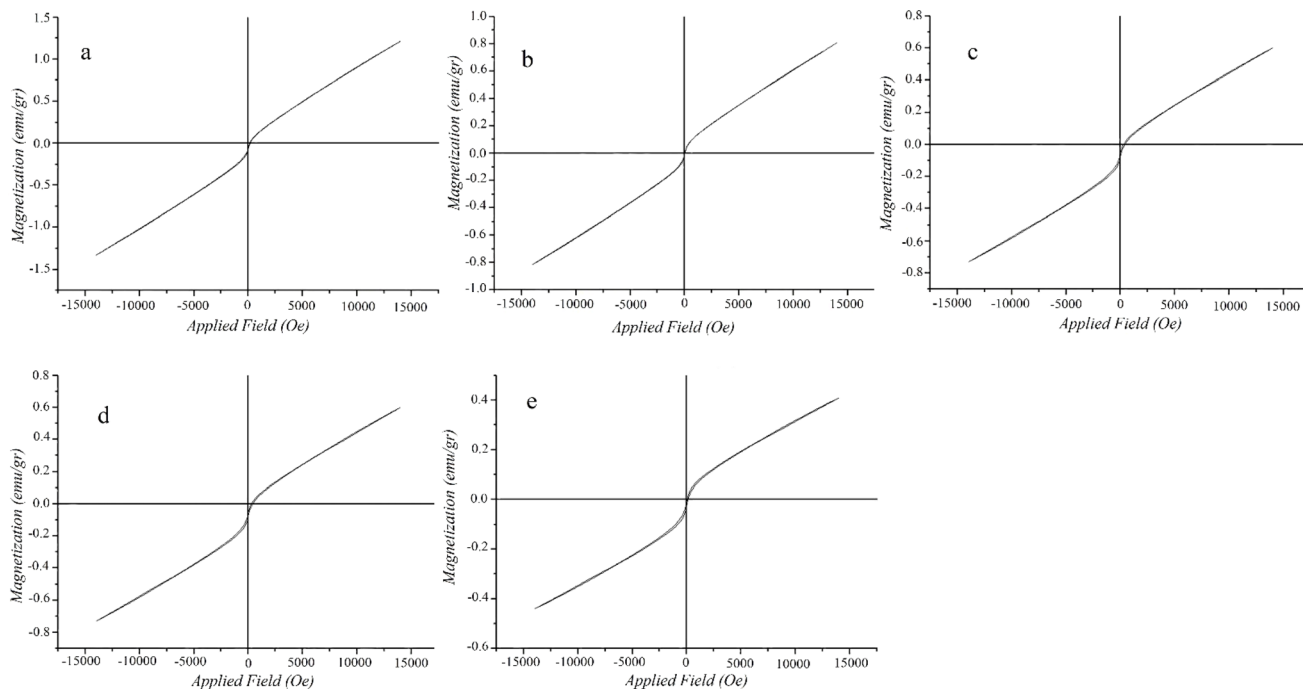
Fig. 7 Hysteresis loops of (a) NPs, (b) SCNPs, (c) CPTMS/SCNPs, (d) DETA/CPTMS/SCNPs, (e) Mg–Al LDH/DETA/CPTMS/SCNPs composite at room temperature using VSM. Reaction conditions: (a) $FeCl_3 \cdot 6H_2O$ (1.8 g), $MnSO_4 \cdot H_2O$ (2.55 g), deionized water (150 mL), under N_2 gas, NaOH 8 M, pH 10, 80 °C, 3 h. (b) $MnFe_2O_4$ (6 g), 0.1 M HCl (100 mL), ultrasonic irradiation, 40 mL deionized water, ethanol (100 mL), 28% ammonia aqueous solution (15 mL), TEOS (20 mL), r.t., 8 h. (c) SCNPs (2 g), 3-chloropropyl trimethoxysilane (60 mL), dry toluene (50 mL), under N_2 gas, 60 °C, 48 h. (d) CPTMS/SCNPs (2 g), dry toluene (50 mL), diethylenetriamine (60 mL), under reflux, under N_2 gas, 48 h. (e) 0.1 M $AlCl_3 \cdot 6H_2O$ (10 mL), 0.3 M $MgCl_2 \cdot 6H_2O$ (10 mL), 0.15 M NaOH (40 mL), autoclave, 100 °C, 24 h, DETA/CPTMS/SCNPs (1 g), 60 °C for 24 h.
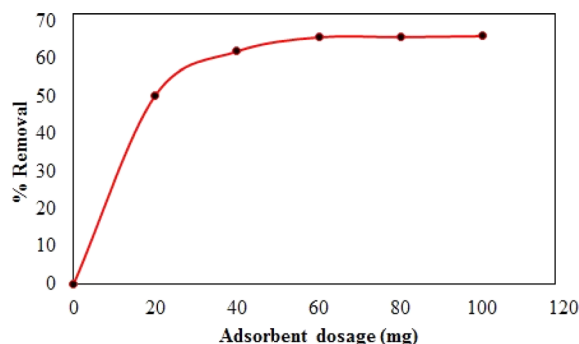

Fig. 8 Effect of adsorbent dosage on percentage of removal of tetracycline (200 rpm, 25 °C, pH = 7, 10 min, initial drug concentrations 100 mg L^{-1}).
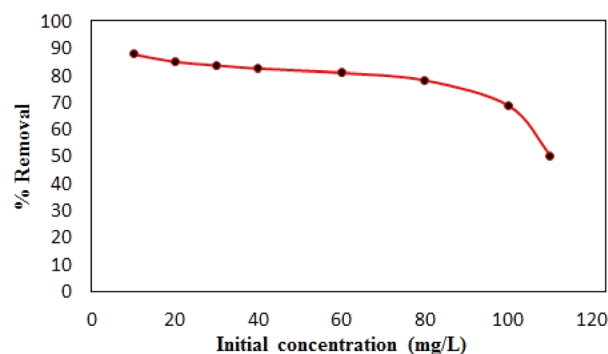

Fig. 9 Effect of initial drug concentration on percentage of removal of tetracycline (200 rpm, 25 °C, pH = 7, 10 min, initial drug concentrations 100 mg L^{-1}).

K_F and n are experimental constants where K_F is adsorption capacity at unit concentration (L mg^{-1}) and n shows the intensity of adsorption. The $1/n$ values can be classified as irreversible ($1/n = 0$), favorable ($0 < 1/n < 1$) and unfavorable ($1/n > 1$). The values of K_F and n were determined from the intercept and slope of the plot of $\ln q_e$ *versus* $\ln C_e$ at 25 °C (Fig. 14). Furthermore, the dimensionless separation factor (R_L) was calculated by the following eqn (6):

$$R_L = \frac{1}{1 + K_L \times C_0} \qquad (6)$$

The values of R_L can demonstrate the shape of the isotherm to be either unfavorable ($R_L > 1$), linear ($R_L = 1$), favorable ($0 < R_L < 1$) or irreversible ($R_L = 0$).

The Temkin adsorption isotherm directly investigates account of adsorbent–adsorbate interactions. In this model, first, heat of adsorption would decrease linearly rather than logarithmic, then uniform distribution of binding energies up to some maximum binding energy.[49] Eqn (7) and (8) show the Temkin isotherm model:
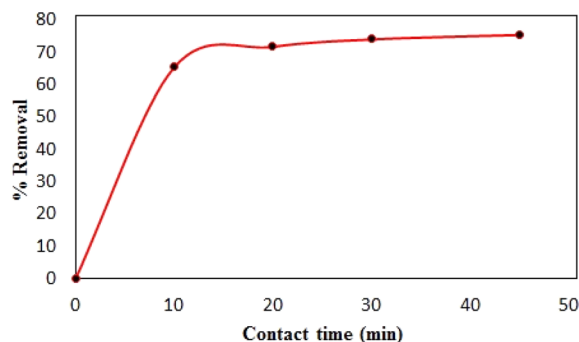
$$q_e = B \ln A + B \ln C_e \qquad (7)$$

Fig. 10 Effect of contact time on percentage of removal of tetracycline (200 rpm, 25 °C, pH = 7, initial drug concentrations 100 mg L^{-1}).
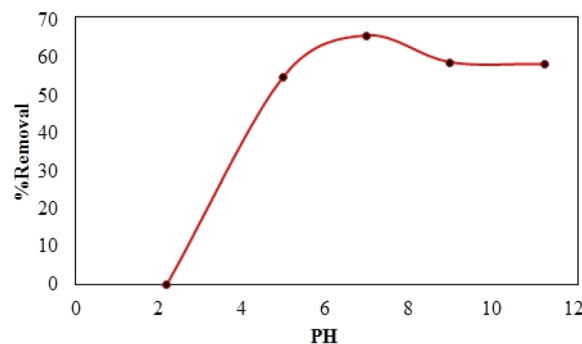

Fig. 12 Effect of pH solution on percentage of removal of tetracycline (200 rpm, 25 °C, 60 mg adsorbent, initial drug concentrations 100 mg L^{-1}).

$$B = \frac{RT}{b} \qquad (8)$$

where R is gas constant 8.314 J mol^{-1} K^{-1}. T is absolute temperature (K), b is the Temkin constant related to the heat of adsorption (J mol^{-1}) and A is the equilibrium binding constant corresponding to the maximum binding energy (L g^{-1}). The values of A and b can be determined from the intercept and slope of the linear plot of q_e *versus* ln C_e (Fig. 15). The Langmuir, Freundlich and Temkin parameters and the regression coefficients R^2 of the adsorption of tetracycline onto Mg–Al LDH/DETA/CPTMS/SCNPs composite are given in Table 1. As seen in Table 1, calculated amount of R_L was found between 0 and 1, which confirmed a favorable adsorption process for tetracycline removal using Mg–Al LDH/DETA/CPTMS/SCNPs composite. Also according to Table 1, the correlation coefficient (R^2) of the Langmuir isotherm was greater than that of the Freundlich and Temkin isotherm models for the adsorption of investigated drug. The applicability of the Langmuir model suggests homogeneous surfaces of the composite and monolayer coverage of tetracycline onto the adsorbent. On the basis of the Langmuir analysis, the maximum adsorption capacity was 40.12 mg g^{-1} for tetracycline.

3.2.6. Adsorption kinetics. In the present study, in order to examine the mechanism of adsorption of drug, two kinetic models, namely, pseudo-first order and pseudo-second order were used to fit the experimental data.[50,51] The linear equation of pseudo-first-order and pseudo-second-order kinetic are given by (9) and (10) equations, respectively:
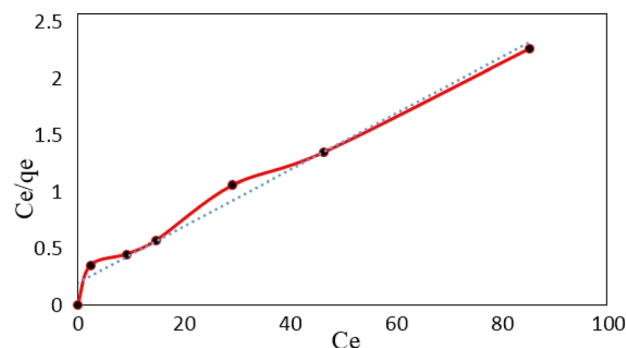

Fig. 13 Langmuir plot for the adsorption of tetracycline (200 rpm, 25 °C and pH = 7).
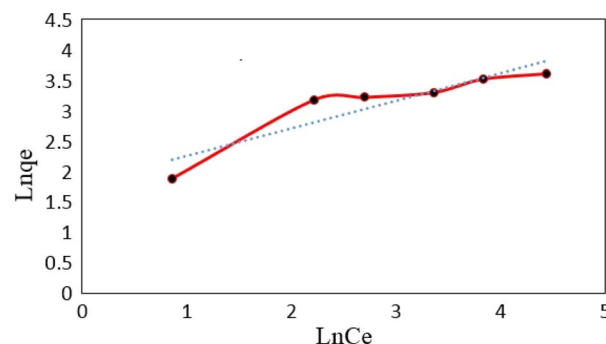

Fig. 14 Freundlich plot for the adsorption of tetracycline (200 rpm, 25 °C and pH = 7).
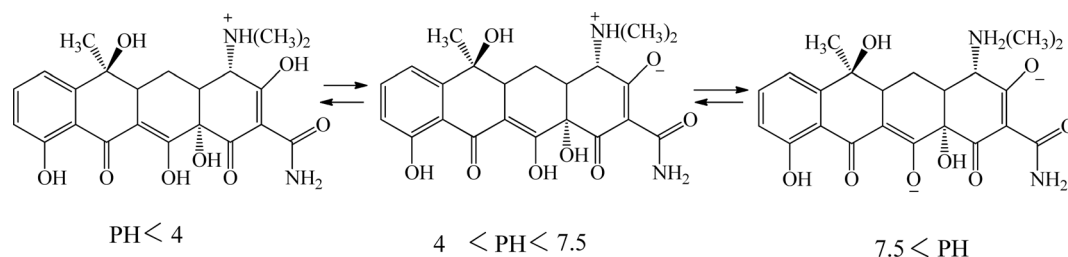

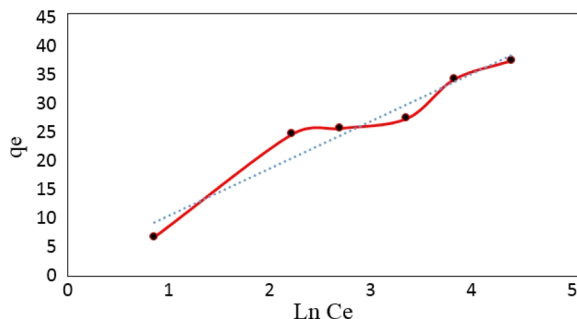**Fig. 11** Effect of pH on structure of tetracycline.

Fig. 15 Temkin plot for the adsorption of tetracycline (200 rpm, 25 °C and pH = 7).

$$\log(q_e - q_t) = \log q_e - \frac{K_1}{2.303} t \qquad (9)$$

$$\frac{t}{q_t} = \frac{1}{K_2 q_e^2} + \frac{t}{q_e} \qquad (10)$$

where q_e and q_t (mg g^{-1}) is the amount of drug adsorbed at equilibrium and at time t, K_1 and K_2 (min^{-1}) are the rate constants. According to eqn (9) and (10), the adsorption data gained in the present study plotted for composite are shown in Fig. 16. The values of rate constant K_1 and q_e are calculated from the straight line plots of $\log(q_e - q_t)$ *vs.* time in the pseudo-first-order model (Fig. 16a). The values of first order rate constant (K_1) was obtained as 0.0072 min^{-1}, calculated removal capacity (q_e) as 17.86 (mg g^{-1}) and coefficient of linear regression (R^2) as 0.9721. The pseudo second order constants can be calculated from the linear plot between t/q_t and time which is given in

Fig. 16b. The values of K_2, q_e and R^2 were obtained 0.034 min^{-1}, 23.26 mg g^{-1} and 0.9992, respectively. The q_e value obtained by calculating pseudo second order kinetic is close to the experimental value (36.80), also the pseudo second order model has high regression coefficient ($R^2 = 0.9992$) than the pseudo first order ($R^2 = 0.9721$).

3.2.7. Thermodynamic studies. Thermodynamic factors such as Gibbs free energy change ($\Delta G°$), enthalpy change ($\Delta H°$) and entropy change ($\Delta S°$) were calculated in temperature range of 298–330 K. The thermodynamic factors were calculated from experimental data using following eqn (11) and (12):

$$\text{Ln } K_C = \frac{\Delta S°}{R} - \frac{\Delta H°}{RT} \qquad (11)$$

$$\Delta G° = \Delta H° - T\Delta S° \qquad (12)$$

where K_C is the thermodynamic equilibrium constant of adsorption (mg L^{-1}), T is the solution temperature and R is the universal gas constant (8.314 J mol^{-1} K^{-1}). The enthalpy ($\Delta H°$) and entropy ($\Delta S°$) changes of adsorption can be determined by the slope and intercept of the plot of ln K_C *versus* $1/T$ (Fig. 17). In addition, the values of $\Delta G°$ at different temperatures are calculated by eqn (12). Table 2 shows a summary of obtained $\Delta G°$, $\Delta H°$ and $\Delta S°$. As it can be observed in Table 2, the obtained positive $\Delta H°$ value of enthalpy (38.93) indicate that the adsorption of tetracycline on Mg–Al LDH/DETA/CPTMS/SCNPs composite is an endothermic process.[52] The negative values in the change of Gibbs free energy ($\Delta G°$) are showing that the investigated process is spontaneous and feasible.[53] The obtained value of $\Delta S°$ of 0.168 kJ mol^{-1} K^{-1} suggests that the

Table 1 Langmuir, Freundlich and Temkin isotherms parameters and correlation coefficients for the adsorption of tetracycline onto Mg−Al LDH/DETA/CPTMS/SCNPs composite

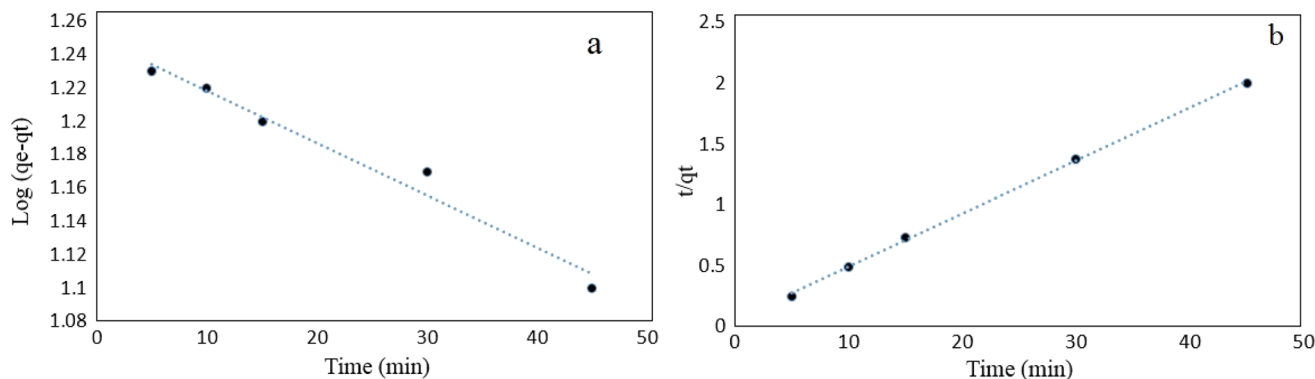| Langmuir isotherm parameters				Freundlich isotherm parameters			Temkin isotherm parameters			
q_m (mg g^{-1})	K_L (L mg^{-1})	R_L	R^2	K_F (L mg^{-1})	n	R^2	A	b (kJ mol^{-1})	B	R^2
40.12	0.125	0.13	0.982	66.06	2.23	0.841	1.86	0.301	8.23	0.9434

Fig. 16 Pseudo-first-order (a) and pseudo-second-order (b) model for the removal kinetics of tetracycline on Mg−Al LDH/DETA/CPTMS/SCNPs composite (200 rpm, 25 °C and pH = 7).
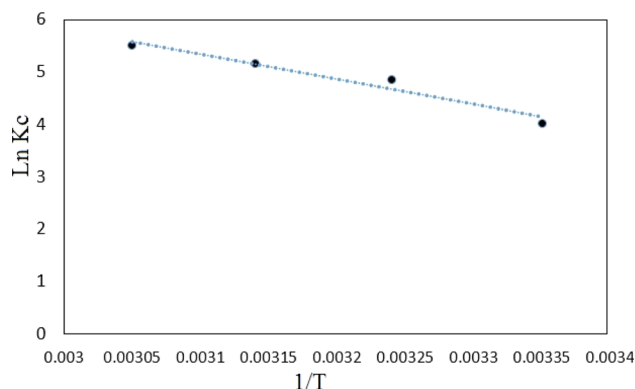
Fig. 17 Thermodynamic plot for removal of tetracycline on Mg–Al LDH/DETA/CPTMS/SCNPs composite (200 rpm, 25 °C and pH = 7).

Fig. 18 Mechanism of tetracycline adsorption on Mg–Al LDH/DETA/CPTMS/SCNPs composite.

increased randomness at the solid/solution interface during the tetracycline on Mg–Al LDH/DETA/CPTMS/SCNPs composite.

3.3. Adsorption mechanism

The adsorption mechanism of tetracycline on the absorbent surface depends on factors such as drug nature, adsorbent properties, hydrogen bonding, electrostatic interaction, π–π interaction and van der Waals forces.[54] The functional groups on tetracycline and Mg–Al LDH/DETA/CPTMS/SCNPs composite can be protonated or deprotonated through pH changes of the aqueous medium. At low pH (acidic environment), due to the pH effect both compounds have a positive charge and the competition of H^+ ions results in less adsorption tendency of tetracycline.[55] In the neutral or alkaline environment, the tetracycline is deprotonated. Therefore, the tetracycline molecule was adsorbed by Mg–Al LDH/DETA/CPTMS/SCNPs composite through hydrogen bonding and electrostatic interaction (Fig. 18).

3.4. Reusability studies

Reusability is one of the important factors from the cost point of view in studying the adsorption process in water treatment. To examine the regeneration ability of the Mg–Al LDH/DETA/CPTMS/SCNPs composite, four cycle of antibiotic removal were investigated. Fig. 19 present the results of this evaluation. For this aim, 60 mg of adsorbent was added to the solution containing 40 mL of 100 mg per L antibiotic. The
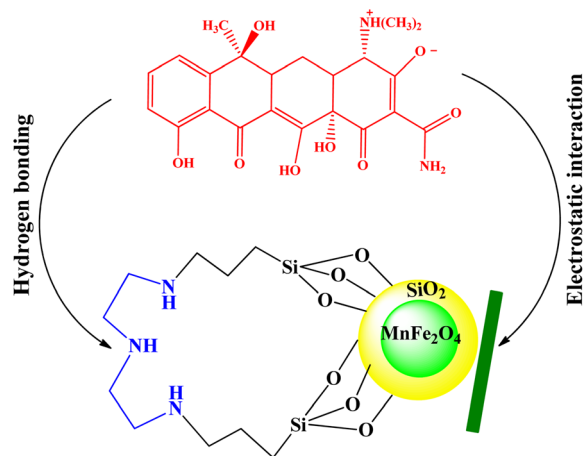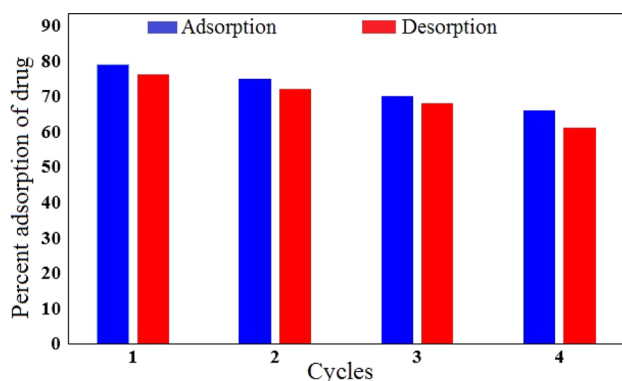

Fig. 19 Regeneration studies for the adsorption–desorption of tetracycline onto Mg–Al LDH/DETA/CPTMS/SCNPs composite.

sample was stirred for 30 min under 200 rpm at 298 K, then was filtered. The adsorbent was washed with deionized water and ethanol several. The Fig. 19 shows that after four cycles, the drug removal percentage decreased slightly and was still 61%. This suggested that the Mg–Al LDH/DETA/CPTMS/SCNPs composite is efficient for tetracycline.

3.5. Comparison with other reported adsorbents

Table 3 demonstrates the result which is gained through comparison of this adsorbent with other established adsorbents.

Table 2 Thermodynamic data for removal of tetracycline onto Mg–Al LDH/DETA/CPTMS/SCNPs composite at different temperatures

Drug	Temperature (K)	Parameters		
		$\Delta G°$ (kJ mol^{-1})	$\Delta H°$ (kJ mol^{-1})	$\Delta S°$ (kJ mol^{-1} K^{-1})
Tetracycline	297	−11.13	38.93	0.168
	308	−12.81		
	318	−14.49		
	328	−16.17		

Table 3 Comparison of the adsorption capacity of present system with other reported systems for tetracycline adsorption

Adsorbents	T (K)	pH	q_m (mg g^{-1})	References
HAP/ZnO-1	298	5	33.97	56
Biochar	298	7	4.13	57
Silica-composited biochar	298	7	22.5	58
MnFe$_2$O$_4$/rGO	298	3.3	41	59
Fe$_3$O$_4$ nanoparticles	302	7	19.6	60
α-Fe$_3$O$_4$/reduced graphene oxide	298	4	18.47	61
Halloysite/chitosan nanocomposite	298	8.5	15.6	62
Rice husk ash	313	5	8.37	63
Copper/cobalt ferrite@chitosan	298	3.5	4.48	64
Mg–Al LDH/DETA/CPTMS/SCNPs composite	298	7	40.16	Present study

As it is shown in Table 3, the adsorption capacity of Mg–Al LDH/DETA/CPTMS/SCNPs composite is acceptable for removal of tetracycline from aqueous solutions.

4. Conclusion

In the present study, the Mg–Al LDH/DETA/CPTMS/SCNPs composite was prepared *via* modification of MnFe$_2$O$_4$ by tetraethyl orthosilicate, 3-chloropropyl trimethoxysilane, diethylenetriamine and Mg–Al layered double hydroxide. The synthesized composite was characterized by FT-IR, XRD, SEM, VSM and TGA. The composite exhibited magnetic property with a saturation magnetization of 0.40 emu g^{-1}. The Mg–Al LDH/DETA/CPTMS/SCNPs composite was used successfully as an effective sorbent for the removal of tetracycline from aqueous solutions. The effects of different factors such as adsorbent dosage, initial drug concentration, pH and contact time were studied. The optimized variable conditions such as adsorbent dose of 60 mg L^{-1}, drug concentration of 100 mg L^{-1}, pH = 7 and contact time 30 min were obtained. The better fitted Langmuir isotherm model showed that the adsorption of tetracycline on synthesized composite was mainly monolayer adsorption. According to the Langmuir analysis, the maximum adsorption capacity (q_m) of the adsorbent for tetracycline was obtained to be 40.16 mg g^{-1}. The kinetic studies revealed that the adsorption process was more suitable for the pseudo second-order process. The thermodynamic study showed that adsorption of tetracycline on composite was spontaneous and endothermic, which was proceeded *via* hydrogen bonding and electrostatic interaction.

Conflicts of interest

There are no conflicts to declare.

References

1 N. El Messaoudi, Z. Ciğeroğlu, Z. Mine Şenol, A. Bouich, E. S. Kazan-Kaya, L. Noureen, J. H. Pinê Américo-Pinheiro and C. Fourteen, Green synthesis of nanoparticles for remediation organic pollutants in wastewater by adsorption, *Adv. Chem. Pollut., Environ. Manage. Prot.*, 2024, **10**, 305–345, DOI: 10.1016/bs.apmp.2023.06.016.

2 G. R. Boyd, H. Reemtsma, D. A. Grimm and S. Mitra, Pharmaceuticals and personal care products (PPCPs) in surface and treated waters of Louisiana, *Sci. Total Environ.*, 2003, **311**, 135–149, DOI: 10.1016/S0048-9697(03)00138-4.

3 R. Cao, J. Wang, W. Ben and Z. Qiang, The profile of antibiotic resistance genes in pig manure composting shaped by composting stage: mesophilic-thermophilic and cooling maturation stages, *Chemosphere*, 2020, **250**, 126181, DOI: 10.1016/j.chemosphere.2020.126181.

4 Q. Qin, X. Wu, L. Chen, Z. Jiang and Y. Xu, Simultaneous removal of tetracycline and Cu(ii) by adsorption and coadsorption using oxidized activated carbon, *RSC Adv.*, 2018, **8**, 1744–1752, DOI: 10.1039/C7RA12402C.

5 H. Sayğılı and F. Güzel, Effective removal of tetracycline from aqueous solution using activated carbon prepared from tomato (*Lycopersicon esculentum* Mill.) industrial processing waste, *Ecotoxicol. Environ. Saf.*, 2016, **131**, 22–29, DOI: 10.1016/j.ecoenv.2016.05.001.

6 Z. Li, Y. Liu, S. Zou, C. Lu, H. Bai and H. Mu, Removal and adsorption mechanism of tetracycline and cefotaxime contaminants in water by NiFe$_2$O$_4$-COF chitosan-terephthalaldehyde nanocomposites film, *Chem. Eng. J.*, 2020, **382**, 123008, DOI: 10.1016/j.cej.2019.123008.

7 S. Shao and X. Wu, Microbial degradation of tetracycline in the aquatic environment: a review, *Crit. Rev. Biotechnol.*, 2020, **40**, 1010–1018, DOI: 10.1080/07388551.2020.1805585.

8 Z. Mulushewa, W. T. Dinbore and Y. Ayele, Removal of methylene blue from textile waste water using kaolin and zeolite-x synthesized from Ethiopian kaolin, *Environ. Anal. Health Toxicol.*, 2021, **36**, e2021007, DOI: 10.5620/eaht.2021007.

9 S. Wang and H. Wang, Adsorption behavior of antibiotic in soil environment: a critical review, *Front. Environ. Sci. Eng.*, 2015, **9**, 565–574, DOI: 10.1007/s11783-015-0801-2.

10 B. Debnath, M. Majumdar, M. Bhowmik, K. L. Bhowmik, A. Debnath and D. N. Roy, The effective adsorption of tetracycline onto zirconia nanoparticles synthesized by novel microbial green technology, *J. Environ. Manage.*, 2020, **261**, 110235, DOI: 10.1016/j.jenvman.2020.110235.

11 F. Yu, Y. Li, S. Han and J. Ma, Adsorptive removal of antibiotics from aqueous solution using carbon materials, *Chemosphere*, 2016, **153**, 365–385, DOI: **10.1016/ j.chemosphere.2016.03.083**.

12 I. Hasana, D. Bhatiaa, S. Waliaa and P. Singha, Removal of Malachite Green by Polyacrylamide-*g*-Chitosan γ-Fe₂O₃ Nanocomposite-An Application of Central Composite Design, *Groundw. Sustain. Dev.*, 2020, **11**, 100378, DOI: **10.1016/j.gsd.2020.100378**.

13 U. S. Malik, Q. Duan, M. B. K. Niazi, Z. Jahan, U. Liaqat, F. Sher, Y. Gan and H. Hou, Vanillin cross-linked hydrogel membranes interfacial reinforced by carbon nitride nanosheets for enhanced antibacterial activity and mechanical properties, *Chin. Chem. Lett.*, 2023, **34**, 108071, DOI: **10.1016/j.cclet.2022.108071**.

14 T. Rasheed, A. A. Hassan, T. Ahmad, S. Khan and F. Sher, Organic Covalent Interaction-based Frameworks as Emerging Catalysts for Environment and Energy Applications: Current Scenario and Opportunities, *Chem.– Asian J.*, 2023, **18**, e202300196, DOI: **10.1002/asia.202300196**.

15 M. Kh. Azeem, A. Islam, R. Ullah Khan, A. Rasool, M. A. R. Qureshi, M. Rizwan, F. Sher and T. Rasheed, Eco-friendly three-dimensional hydrogels for sustainable agricultural applications: current and future scenarios, *Polym. Adv. Technol.*, 2023, **34**, 3046–3062, DOI: **10.1002/ pat.6122**.

16 W. Li, M. Bilal, A. Kumar Singh, F. Sher, S. Salman Ashraf, M. Franco, J. H. Pinê Américo-Pinheiro and H. M. N. Iqbal, Broadening the Scope of Biocatalysis Engineering by Tailoring Enzyme Microenvironment: A Review, *Catal. Lett.*, 2023, **153**, 1227–1239, DOI: **10.1007/s10562-022-04065-5**.

17 N. El Messaoudi, Z. Ciğeroğlu, Z. Mine Şenol, E. Sena Kazan-Kaya, Y. Fernine, S. Gubernat and Z. Lopicic, Green synthesis of CuFe₂O₄ nanoparticles from bioresource extracts and their applications in different areas: a review, *Biomass Convers. Biorefin.*, 2024, DOI: **10.1007/s13399-023-05264-9**.

18 T. Sakshi, An overview on alginate based bio-composite materials for wastewater remedial, *Mater. Today: Proc.*, 2021, **37**, 3305–3309, DOI: **10.1016/j.matpr.2020.09.120**.

19 T. Ahamad, M. Naushad, T. Al-Shahrani, N. Al-Hokbany and S. M. Alshehri, Preparation of chitosan based magnetic nanocomposite for tetracycline adsorption: kinetic and thermodynamic studies, *Int. J. Biol. Macromol.*, 2020, **147**, 258–267, DOI: **10.1016/j.ijbiomac.2020.01.025**.

20 L. Shao, Z. Ren, G. Zhang and L. Chen, Facile synthesis, characterization of a MnFe₂O₄/activated carbon magnetic composite and its effectiveness in tetracycline removal, *Mater. Chem. Phys.*, 2012, **135**, 16–24, DOI: **10.1016/ j.matchemphys.2012.03.035**.

21 M. Zubair, M. Daud, G. McKay, F. Shehzad and M. A. Al-Harthi, Recent progress in layered double hydroxides (LDH)-containing hybrids as adsorbents for water remediation, *Appl. Clay Sci.*, 2017, **143**, 279–292, DOI: **10.1016/j.clay.2017.04.002**.

22 X. Yuan, Y. Wang, J. Wang, C. Zhou, Q. Tang and X. Rao, Calcined graphene/MgAl-layered double hydroxides for enhanced Cr (VI) removal, *Chem. Eng. J.*, 2013, **221**, 204– 213, DOI: **10.1016/j.cej.2013.01.090**.

23 C. Mengbo, L. Xun, W. Wei, G. Ming, L. Yongsheng and Y. Hongbing, Functionalized Zn/Al N-doped carbon nanocomposites with tunable morphology: synergistic ultrafast low-temperature synthesis and tetracycline adsorption, *Sep. Purif. Technol.*, 2021, **278**, 119548, DOI: **10.1016/j.seppur.2021.119548**.

24 S. Mufan, Ch. Zhongjing, Y. Yixuan, H. Bingji, H. Guangyu and Ch. Haiqun, A facile solvothermal syntheses of NiFe layered double hydroxide-Bi₂MoO₆ heterostructure/reduced graphene oxide with efficient photodegradation for tetracycline, *Environ. Res.*, 2022, **204**, 112037, DOI: **10.1016/ j.envres.2021.112037**.

25 A. Zaher, M. Taha and R. Khaled Mahmoud, Possible adsorption mechanisms of the removal of tetracycline from water by La-doped Zn-Fe-layered double hydroxide, *J. Mol. Liq.*, 2021, **322**, 114546, DOI: **10.1016/ j.molliq.2020.114546**.

26 A. El Guerraf, S. Ben Jadi, I. Ziani, M. Dalli, F. Sher, M. Bazzaoui and El A. Bazzaoui, Multifunctional Smart Conducting Polymers–Silver Nanocomposites-Modified Biocellulose Fibers for Innovative Food Packaging Applications, *Ind. Eng. Chem. Res.*, 2023, **62**, 4540–4553, DOI: **10.1021/acs.iecr.2c01327**.

27 V. Ghobadifar, Gh. Bagheri Marandi, M. Kurdtabar and Gh. Rezanejade Bardajee, Removal of Pb(II) and Cd(II) by MnFe₂O₄@SiO₂@VTMS Nanocomposite Hydrogel from Aqueous Solutions, *J. Polym. Environ.*, 2023, **31**, 2686–2704, DOI: **10.1007/s10924-022-02670-4**.

28 Z. Rashid, H. Naeimi and A. H. Zarnani, Fast and highly efficient purification of 6× histidine-tagged recombinant proteins by Ni-decorated MnFe₂O₄@SiO₂@NH₂@2AB as novel and efficient affinity adsorbent magnetic nanoparticles, *RSC Adv.*, 2016, **6**, 36840–36848, DOI: **10.1039/C5RA25949E**.

29 Z. P. Xu, G. Stevenson, C. Q. Lu, G. Q. Lu, P. F. Bartlett and P. Gray, Stable suspension of layered double hydroxide nanoparticles in aqueous solution, *J. Am. Chem. Soc.*, 2006, **128**, 36–37, DOI: **10.1021/ja056652a**.

30 M. Ghobadi, M. Gharabaghi, H. Abdollahi, Z. Boroumand and M. Moradian, MnFe₂O₄-graphene oxide magnetic nanoparticles as a high-performance adsorbent for rare earth elements: synthesis, isotherms, kinetics, thermodynamics and desorption, *J. Hazard. Mater.*, 2018, **351**, 308–316, DOI: **10.1016/j.jhazmat.2018.03.011**.

31 N. U. Yamaguchi, R. Bergamasco and S. Hamoudi, Magnetic MnFe₂O₄–graphene hybrid composite for efficient removal of glyphosate from water, *Chem. Eng. Sci.*, 2016, **295**, 391– 402, DOI: **10.1016/j.cej.2016.03.051**.

32 F. Adam, H. Osman and K. M. Hello, The immobilization of 3-(chloropropyl)triethoxysilane onto silica by a simple one-pot synthesis, *J. Colloid Interface Sci.*, 2009, **331**, 143–147, DOI: **10.1016/j.jcis.2008.11.048**.

33 A. Kaczmarek, J. Hoffman, J. Morgiel, T. Mościcki, L. Stobiński, Z. Szymański and A. Małolepszy, Luminescent Carbon Dots Synthesized by the Laser Ablation of Graphite

in Polyethylenimine and Ethylenediamine, *Materials*, 2021, **14**, 729, DOI: **10.3390/ma14040729**.

34 J. Li, Y. Wang, S. Jiang and H. Zhang, Facile synthesis of magnetic recyclable palladium-gold alloy nanoclusters catalysts PdAur/Fe$_3$O$_4$@LDH and its catalytic applications in Heck reaction, *J. Organomet. Chem.*, 2018, **878**, 84–95, DOI: **10.1016/j.jorganchem.2018.10.007**.

35 F. Mi, X. Chen, Y. Ma, S. Yin, F. Yuan and H. Zhang, Facile synthesis of hierarchical core–shell Fe$_3$O$_4$@MgAl-LDH@Au as magnetically recyclable catalysts for catalytic oxidation of alcohols, *Chem. Commun.*, 2011, **47**, 12804–12806, DOI: **10.1039/C1CC15858A**.

36 Y. Xiao, J. Zai, L. Tao, B. Li, Q. Han, C. Yu and X. Qian, MnFe$_2$O$_4$–graphene nanocomposites with enhanced performances as anode materials for Li-ion batteries, *Phys. Chem. Chem. Phys.*, 2013, **15**, 3939–3945, DOI: **10.1039/C3CP50220A**.

37 Z. Rezvani, F. Arjomandi Rad and F. Khodam, Synthesis and characterization of Mg–Al-layered double hydroxides intercalated with cubane1,4-dicarboxylate anions, *Dalton Trans.*, 2015, **44**, 988–996, DOI: **10.1039/C4DT03152K**.

38 Li. Tianxiang, Sh. Zhengren, He. Xianru, J. Ping, Lu. Xiaobin, R. Zhang and X. Wang, Aging-resistant functionalized ldh–sas/nitrile-butadiene rubber composites: preparation and study of aging kinetics/anti-aging mechanism, *Materials*, 2018, **11**, 836, DOI: **10.3390/ma11050836**.

39 S. N. Golovin, M. N. Yapryntsev, I. G. Ryl'tsova, S. V. Savilov, K. I. Maslakov and O. E. Lebedeva, Synthesis and thermal behavior of Co/AlCe layered double hydroxide, *Solid State Sci.*, 2021, **111**, 106498, DOI: **10.1016/j.solidstatesciences.2020.106498**.

40 Y. Zhang, Li. Lijuan, Sh. Dong and F. Song, Synthesis and application of low-cost layered double hydroxides intercalated by gluconic acid anion for flame retardancy and tensile strength conservation of high filling epoxy resin, *J. Colloid Interface Sci.*, 2021, **594**, 791–801, DOI: **10.1016/j.jcis.2021.03.088**.

41 A. A. Ali Ahmed, Z. A. Talib and M. Z. Hussein, Thermal, optical and dielectric properties of Zn–Al layered double hydroxide, *Appl. Clay Sci.*, 2012, **56**, 68–76, DOI: **10.1016/j.clay.2011.11.024**.

42 L. Gui-yin, J. Jiang Yu-ren, K. Huang, P. Ding and J. Chen, Preparation and properties of magnetic Fe$_3$O$_4$–chitosan nanoparticles, *J. Alloys Compd.*, 2008, **466**, 451–456, DOI: **10.1016/j.jallcom.2007.11.100**.

43 R. Hosseinzadeh, M. Mavvaji and I. Moradi, Synthesis and Characterization of Fe$_3$O$_4$@SiO$_2$@MgAl-LDH@Au.Pd as an Efficient and Magnetically Recyclable Catalyst for Reduction of 4-Nitrophenol and Suzuki Coupling Reactions, *Arabian J. Sci. Eng.*, 2023, **48**, 7525–7541, DOI: **10.1007/s13369-022-07543-5**.

44 W. Honghai, X. Hanrui, H. Guangping, Y. Guan and Y. Zhang, Effects of the pH and anions on the adsorption of tetracycline on iron-montmorillonite, *Appl. Clay Sci.*, 2016, **119**, 161–169, DOI: **10.1016/j.clay.2015.08.001**.

45 Zh. Yanping, G. Xueyuan, G. Shixiang, J. Geng and X. Wang, Adsorption of tetracycline (TC) onto montmorillonite:

46 A. Saadat, A. Banaei, M. Sattarifar and P. Pargolghasemi, Preparation 2-hydroxy-1-naphthaldehyde cross-linked Fe$_3$O$_4$@chitosan-polyacrylamide nanocomposite for removal of everzol black from aqueous solutions, *Sci. Rep.*, 2023, **13**, 10618, DOI: **10.1038/s41598-023-37243-5**.

47 A. Tabak, E. Eren, B. Afsin and B. Caglar, Determination of adsorptive properties of a Turkish Sepiolite for removal of Reactive Blue 15 anionic dye from aqueous solutions, *J. Hazard. Mater.*, 2009, **161**, 1087–1094, DOI: **10.1016/j.jhazmat.2008.04.062**.

48 R. Satheesh, K. Vignesh, M. Rajarajan, A. Suganthi, S. Sreekantan, M. Kang and B. Sub Kwak, Removal of congo red from water using quercetin modified α-Fe$_2$O$_3$ nanoparticles as effective nanoadsorbent, *Mater. Chem. Phys.*, 2016, **180**, 53–65, DOI: **10.1016/j.matchemphys.2016.05.029**.

49 N. Wang, J. Chen, J. Wang, J. Feng and W. Yan, Removal of Methylene Blue by Polyaniline/TiO$_2$ Hydrate: Adsorption Kinetic, Isotherm and Mechanism Studies, *Powder Technol.*, 2019, **347**, 93–102, DOI: **10.1016/j.powtec.2019.02.049**.

50 S. X. Chen, J. Wang, Z. L. Wu, Q. Deng, W. F. Tu, G. P. Dai, Z. L. Zeng and S. G. Deng, Enhanced Cr(VI) removal by polyethylenimine and phosphorus codoped hierarchical porous carbons, *J. Colloid Interface Sci.*, 2018, **523**, 110–120, DOI: **10.1016/j.jcis.2018.03.057**.

51 A. A. Alqadami, M. Naushad, M. A. Abdalla, M. R. Khan and Z. A. Alothman, Adsorptive removal of toxic dye using Fe$_3$O$_4$–TSC nanocomposite: equilibrium, kinetic and thermodynamic studies, *J. Chem. Eng. Data*, 2016, **61**, 3806–3813, DOI: **10.1021/acs.jced.6b00446**.

52 R. Shan, L. Yan, K. Yang, S. Yu, Y. Hao, H. Yu and B. Du, Magnetic Fe$_3$O$_4$/MgAl-LDH composite for effective removal of three red dyes from aqueous solution, *J. Chem. Eng.*, 2014, **252**, 38–46, DOI: **10.1016/j.cej.2014.04.105**.

53 Y. Jiang, B. Liu, J. Xu, K. Pan, H. Hou, J. Hu and J. Yang, Cross-linked chitosan/β-cyclodextrin composite for selective removal of methyl orange: adsorption performance and mechanism, *Carbohydr. Polym.*, 2018, **182**, 106–114, DOI: **10.1016/j.carbpol.2017.10.097**.

54 R. Natarajan, K. Saikia, S. K. Ponnusamy, A. K. Rathankumar, D. S. Rajendran, S. Venkataraman, D. B. Tannani, V. Arvind, T. Somanna, K. Banerjee, N. Mohideen and V. K. Vaidyanathan, Understanding the factors affecting adsorption of pharmaceuticals on different adsorbents- a critical literature update, *Chemosphere*, 2022, **287**, 131958, DOI: **10.1016/j.chemosphere.2021.131958**.

55 H. Zhu, T. Chen, J. Liu and D. Li, Adsorption of tetracycline antibiotics from an aqueous solution onto graphene oxide/calcium alginate composite fibers, *RSC Adv.*, 2018, **8**, 2616–2621, DOI: **10.1039/C7RA11964J**.

56 C. Oliveira, A. L. M. de Oliveira, L. Chantelle, R. Landers, S. Medina-Carrasco, M. Del Mar Orta, E. C. Silva Filho and M. G. Fonseca, Zinc(II) modified hydroxyapatites for

tetracycline removal: Zn(II) doping or ZnO deposition and their influence in the adsorption, *Polyhedron*, 2021, **194**, 114879, DOI: **10.1016/j.poly.2020.114879**.

57 Y. Dai, J. Li and D. Shan, Adsorption of tetracycline in aqueous solution by biochar derived from waste *Auricularia auricula* dregs, *Chemosphere*, 2020, **238**, 124432, DOI: **10.1016/j.chemosphere.2019.124432**.

58 Z. Zhao, T. Nie and W. Zhou, Enhanced biochar stabilities and adsorption properties for tetracycline by synthesizing silica-composited biochar, *Environ. Pollut.*, 2019, **254**, 113015, DOI: **10.1016/j.envpol.2019.113015**.

59 W. A. Khanday and B. H. Hameed, Zeolite-hydroxyapatite-activated oil palm ash composite for antibiotic tetracycline adsorption, *Fuel*, 2018, **215**, 499–505, DOI: **10.1016/j.fuel.2017.11.068**.

60 W. Zhai, J. He, P. Han, M. Zeng, X. Gao and Q. He, Adsorption mechanism for tetracycline onto magnetic Fe_3O_4 nanoparticles: adsorption isotherm and dynamic behavior, location of adsorption sites and interaction bonds, *Vacuum*, 2022, **195**, 110634, DOI: **10.1016/j.vacuum.2021.110634**.

61 A. M. Huízar-Félix, C. Aguilar-Flores, A. Martínez-de-la Cruz, J. M. Barandiarán, S. Sepúlveda-Guzmán and R. Cruz-Silva, Removal of tetracycline pollutants by adsorption and magnetic separation using reduced graphene oxide decorated with α-Fe_2O_3 nanoparticles, *Nanomaterials*, 2019, **9**, 313, DOI: **10.3390/nano9030313**.

62 S. Erdem, M. Öztekin and Y. S. Açıkel, Investigation of tetracycline removal from aqueous solutions using halloysite/chitosan nanocomposites and halloysite nanotubes/alginate hydrogel beads, *Environ. Nanotechnol., Monit. Manage.*, 2021, **16**, 100576, DOI: **10.1016/j.enmm.2021.100576**.

63 Y. Chen, F. Wang, L. Duan, H. Yang and J. Gao, Tetracycline adsorption onto rice husk ash, an agricultural waste: its kinetic and thermodynamic studies, *J. Mol. Liq.*, 2016, **222**, 487–494, DOI: **10.1016/j.molliq.2016.07.090**.

64 A. Nasiri, S. Rajabi, A. Amiri, M. Fattahizade, O. Hasani, A. Lalehzari and M. Hashemi, Adsorption of tetracycline using $CuCoFe_2O_4$@chitosan as a new and green magnetic nanohybrid adsorbent from aqueous solutions: isotherm, kinetic and thermodynamic study, *Arabian J. Chem.*, 2022, **15**, 104014, DOI: **10.1016/j.arabjc.2022.104014**.